Sensitivity of SDOF steel-plate response to equivalent pressure-time histories for vented deflagration loads

Francesco Pinna[1], Marco Zucca[2], Marco Simoncelli[3]
[1, 2]Department of Civil and Environmental Engineering and Architecture, University of Cagliari, Via Marengo 2, 09123, Cagliari, Italy
[3]Department of Architecture, Built Environment and Construction Engineering, Politecnico di Milano, Via G. Ponzio 31, 20133, Milano, Italy
[1]Corresponding author
E-mail: [1]*francesco.pinna4@unica.it*, [2]*marco.zucca2@unica.it*, [3]*marco.simoncelli@polimi.it*

Received 12 February 2026; accepted 17 March 2026; published online 22 April 2026
DOI https://doi.org/10.21595/vp.2026.26118

75th International Conference on Vibroengineering in Trieste, Italy, April 13, 2026

Abstract. This paper investigates how the assumed pressure-time shape for vented dust deflagrations affects the predicted dynamic response of thin steel plates using a bilinear SDOF model with Cowper-Symonds strain-rate effects. Five peak/impulse-matched, peak-aligned equivalent load laws triangular, right-triangle, reversed Friedlander, double reversed Friedlander, and a hybrid ramp and tail are compared against a CFD-validated reference trace. Results quantify sensitivity of mid-span deflection and peak demand to rise/decay assumptions, identifying when impulse matching is sufficient and when rise time and post-peak tail must be modeled explicitly.

Keywords: SDOF model, steel plate, vented deflagration, equivalent load, pressure-time history, impulse.

1. Introduction

Vented dust deflagrations remain a critical safety scenario for industrial enclosures, filtration units, and lightweight casings [1]. Although venting limits the peak overpressure, it does not remove the transient pressure loading acting on structural panels, whose rise times and decay tails can differ markedly from classical blast waveforms and introduce additional uncertainty beyond the reduced-pressure magnitude alone. In engineering practice, simplified equivalent pressure-time shapes are often adopted for rapid plate assessments. The consequences of the selected idealization are rarely discussed explicitly, despite their potential influence on displacement demand, peak-response timing, and, in the inelastic range, permanent deformation.

Single-degree-of-freedom (SDOF) models offer an effective compromise between mechanical fidelity and computational efficiency for preliminary plate-response screening [2]. If the load duration is very short compared with the natural period, impulse equivalence may be sufficient, and different shapes with the same impulse tend to produce similar peak deflections. However, vented deflagration transients often exhibit longer effective durations and nontrivial rise/decay features, making the response sensitive to how the load is distributed in time [3-7], especially when the duration becomes comparable to the structural period. In this regime, identical global descriptors may still produce different dynamic amplification and inelastic demand [8].

Within this context, the present study proposes a practical and reproducible framework for simplifying vented-deflagration pressure loads into a compact set of equivalent pressure-time histories tailored to rapid structural assessment. Rather than relying on a single surrogate waveform, the approach organizes and compares a family of low-parameter idealizations, ranging from triangular pulses to Friedlander-type decay laws [9] and reverse-Friedlander-like profiles able to represent slower pressure build-up followed by vent-controlled decay. The objective is to provide a rational basis for selecting an equivalent representation of vented-deflagration loading according to the response features that must be preserved. The paper then presents the SDOF model and assumptions, defines the load families and matching criteria, discusses response trends

across representative duration-to-period ratios, and concludes with practical guidance for the rapid assessment of plate-like components subjected to vented deflagration loading.

2. SDOF model for blast-loaded steel plates

In this work the plate response is approximated through a reduced-order single-degree-of-freedom (SDOF) formulation in which the full flexural field is condensed into a single generalized displacement $U(t)$associated with the dominant deformation mode [10]. The approach follows the classical plate-to-SDOF idealization for impulsive loads and extends it by (i) a bilinear elastic-plastic resistance, (ii) rate-dependent steel yield stress, and (iii) an explicit time-marching scheme suitable for large batches of simulations.

Let $w(x, y, t)$ be the transverse displacement of a rectangular plate of plan dimensions $a \times b$ and thickness h. The plate kinematics are expressed as a separable approximation $w(x, y, t) = \phi(x, y) \cdot U(t)$, where $\phi(x, y)$ is an assumed mode shape consistent with the boundary conditions, and $U(t)$ is the generalized coordinate representing the mid-span response. The condensed equation of motion is written as:

$$M_e \cdot \ddot{U}(t) + C_e \cdot \dot{U}(t) + R \cdot \left(U(t), \dot{U}(t)\right) = F_e(t), \tag{1}$$

where M_e is the equivalent (lumped) mass, C_e is the equivalent viscous damping, which is neglected here because very short impulses are considered [11], $R(\cdot)$ is the generalized resistance (nonlinear), and $F_e(t)$ is the equivalent generalized load. In the SDOF mapping, the generalized terms are obtained through mass and load factors (commonly denoted K_M and K_L), so that the external force and the stiffness/resistance can be consistently reduced to the single coordinate. In practice, once K_M and K_L are selected for the chosen $\phi(x, y)$ and boundary condition set, the effective inertia and forcing read $M_e = K_M \cdot M$ and $F_e(t) = K_L \cdot P(t)$.

With M the total plate mass and $P(t)$ the resultant pressure load integrated over the plate area (in our case, for uniform pressure, $P(t) = p(t) \cdot a \cdot b$).

The global resistance is represented by a bilinear force–displacement relationship calibrated to the plate type. In the elastic range, $R(U) = k_1 \cdot U$, with $|U| \leq Y_{S1}$ where $r_{S1} = k_1 Y_{S1}$ is the yield-level generalized resistance. A second displacement level Y_{S2} can be introduced as a "plastic cap" (limit displacement) to stop the integration when the assumed bilinear idealization is no longer valid (or to flag a severe damage/failure state). In the implementation, the active stiffness (and corresponding K_M, K_L) is switched depending on whether $|U|$ is below or above Y_{S1}; this allows the model to mimic the progressive boundary-condition change associated with plastic hinge formation along the edges.

Blast loading produces high strain rates, which increase the apparent yield strength of steel and therefore the plate resistance. The rate sensitivity is introduced through a Cowper-Symonds type amplification of the yield stress [12]: $f_{y,d} = f_y \cdot \left[1 + \left(\frac{\dot{\varepsilon}}{C}\right)^{1/q}\right]$, where f_y is the quasi-static yield strength, $\dot{\varepsilon}$ is an equivalent strain rate, and C, q are material constants (typical values used for structural steels in blast-oriented reduced-order models are $C = 40 \cdot s^{-1}$ and $q = 5$ [11]. The updated $f_{y,d}$ is used at each time step to recompute the generalized yield resistance and, consequently, the current thresholds Y_{S1} and Y_{S2}.

The strain-rate input for Cowper-Symonds is obtained from the curvature-rate associated with the assumed mode. For thin plates, the extreme-fiber longitudinal strain is related to curvature by $\varepsilon(t) = \kappa(t) \cdot \frac{h}{2}$, and $\dot{\varepsilon}(t) = \dot{\kappa}(t) \cdot \frac{h}{2}$.

Because $w(x, y, t) = \phi(x, y) \cdot U(t)$, curvatures scale with $U(t)$ and curvature-rates scale with $\dot{U}(t)$. For a given boundary condition, closed-form expressions of $\phi(x, y)$ lead to explicit curvature-rate relations of the form $\dot{\kappa}(t) = \Gamma \cdot \dot{U}(t)$, where Γ is a geometry- and mode-dependent

constant (e.g., proportional to $(\pi/a)^2$ for common trigonometric modes) [2]. The model uses these relations to estimate $\dot{\varepsilon}(t)$ directly from the current generalized velocity $\dot{U}(t)$, updating $f_{y,d}$ and the bilinear resistance consistently at every time step.

Given the millisecond-scale duration of blast loads, an explicit central-difference scheme is adopted for robustness and computational speed. With time step Δt, displacement is advanced using: $U_{n+1} = 2 \cdot U_n - U_{n-1} + \Delta t^2 \cdot \ddot{U}_n$.

Overall, this SDOF formulation retains the key physical mechanisms governing plate response under impulsive pressure, dominant flexural mode, elastic-plastic transition, and rate-dependent resistance, while remaining computationally light enough to support extensive parametric and probabilistic analyses.

3. Equivalent pressure-time histories for vented dust deflagrations

The structural response of thin plates under internal deflagrations is governed by both the peak overpressure and the time distribution of the impulse [2]. In vented dust explosions a progressive pressure build-up during flame acceleration, a maximum associated with the venting competition, and a subsequent decay that may include oscillations and partial vacuum phases due to vent outflow and system compliance. For this reason, rather than adopting a single canonical blast function, several equivalent pressure-time shapes are considered to reproduce, in a controlled manner, the key descriptors of a vented deflagration curve within a prescribed time window. In all cases, the equivalent load is built to preserve the peak pressure $P_{\max}$ and the impulse I (evaluated over a selected duration t_{end}), while modifying the "shape" of the rise/decay to explore its influence on the SDOF response [13].

In the following $p(t)$ denotes the measured/simulated vented-deflagration pressure (reference curve), $P_{\max} = \max p(t)$ is the peak within the chosen window [0, t_{end}], and $I = \int_0^{t_{end}} p(t) \cdot dt$ is the corresponding net impulse. Each equivalent law $p_{eq}(t)$ is defined to remain non-negative, i.e. $p_{eq}(t) \geq 0$, and the calibration of the equivalent shapes is performed against the positive-phase descriptors $P_{\max}$ and I over [0, t_{end}]. The time alignment is performed such that the peak of p_{eq} is centered on the peak time of the reference curve, ensuring a meaningful comparison of rise rate and post-peak decay.

The simplest representation of a vented deflagration build-up is a monotonic ramp reaching $P_{\max}$ at the peak time t_p, followed by an instantaneous drop to zero [14]. This "right-triangle" model isolates the effect of a progressive pressurization without post-peak tail and is particularly useful to test the sensitivity of the SDOF response to the rise segment alone. The equivalent law is defined as:

$$p_{RT}(t) = \begin{cases} P_{\max} \cdot \dfrac{t - (t_p - \tau)}{\tau}, & t_p - \tau \leq t \leq t_p, \\ 0, & \text{otherwise}, \end{cases} \tag{2}$$

where τ is selected to enforce impulse matching. Because the area is triangular, $I = \frac{1}{2} \cdot P_{\max} \cdot \tau$ so $\tau = \frac{2 \cdot I}{P_{\max}}$. This model automatically preserves $P_{\max}$ and I, and by construction the peak occurs exactly at $t = t_p$.

To introduce a finite positive phase both before and after the peak, a symmetric triangular pulse is adopted. This shape is representative of cases where pressure increases and decreases with comparable characteristic times, offering a controlled "double-ramp" with zero skewness around the peak.

A convenient definition centered at t_p is:

$$p_{TRI}(t) = \begin{cases} P_{\max} \cdot \left(1 - \dfrac{|t - t_p|}{\tau}\right), & |t - t_p| \le \tau, \\ 0, & \text{otherwise}, \end{cases} \tag{3}$$

where the total base duration is 2τ. The impulse condition gives $\tau = \frac{I}{P_{max}}$. Compared to the right-triangle, this variant distributes the same impulse across a longer support, reducing peak-adjacent slopes and changing the excitation bandwidth experienced by the SDOF oscillator.

External-blast loads are often modeled with a Friedlander pulse (rapid rise, exponential decay), whereas vented dust deflagrations commonly show the opposite asymmetry: a progressive build-up followed by rapid relief once venting dominates. To represent this, a reversed Friedlander-type pulse is adopted, with pressure increasing toward $P_{\max}$ and truncated at a finite end time [6]. A practical normalized form over $[0,\ t_d]$is $p_{RF}(t) = P_{\max} \cdot \left(\frac{t}{t_d}\right) \cdot e^{\left[-\beta \cdot \left(1 - \frac{t}{t_d}\right)\right]}$ and $p_{RF}(t) = 0$ for $t > t_d$. The parameter $\beta > 0$ controls the convexity/concavity of the rise: larger βconcentrates more area closer to the peak, while smaller β produces a more distributed build-up. For a chosen β, impulse matching determines t_d uniquely via $I = \int_0^{t_d} p_{RF}(t) \cdot dt = P_{\max} \cdot t_d \cdot J(\beta)$ where $J(\beta)$ is the closed-form integral of the normalized shape (a constant for a given β). Thus $t_d = \frac{I}{P_{\max} \cdot J(\beta)}$. Finally, the curve is shifted so that its peak occurs at the measured peak time t_p, ensuring direct comparability of the rise segment to the reference deflagration.

Several vented deflagration records exhibit a shoulder or a secondary pressure feature after the main peak, caused by flow reversals, vent-panel dynamics, or multi-compartment interactions. To represent such cases while retaining a limited number of parameters, a "double reversed Friedlander" is considered as the superposition of two reversed-Friedlander lobes with different characteristic durations and weights: $p_{DRF}(t) = A^{(1)}_{p_{RF}}(t; t_{d1}, \beta_1) + (1 - A) \cdot p^{(2)}_{RF} \cdot (t; t_{d2}, \beta_2)$ with each lobe truncated at its own end time and aligned (or slightly delayed) with respect to the primary peak. The parameters $(A, \beta_1, \beta_2, t_{d1}, t_{d2})$ are not all free: the combined signal is calibrated to satisfy global constraints on peak and total impulse over $[0,\ t_{end}]$. In the simplest implementation, the peak is enforced by construction (normalizing both lobes to $P_{\max}$ at t_p), while the impulse constraint is imposed by solving for one unknown duration (e.g., t_{d2}) once the remaining shape parameters are selected.

As a compromise between interpretability and fidelity, a hybrid equivalent load is introduced by combining a deterministic ramp-up (triangular) with a post-peak tail (Friedlander-like). This is motivated by vented deflagration physics: the rise phase is often governed by flame acceleration and dust dispersion (progressive), whereas the post-peak behavior is dictated by vent outflow and gas expansion. A generic piecewise hybrid law can be written as:

$$p_{HYB}(t) = \begin{cases} P_{\max} \cdot \dfrac{t - \left(t_p - \tau_r\right)}{\tau}, & t_p - \tau \le t \le t_p, \\ P_{\max} \cdot e^{\left[-\frac{t - t_p}{\tau_d}\right]}, & t_p < t \le t_{end}, \\ 0, & \text{otherwise}, \end{cases} \tag{4}$$

where τ_r governs the linear build-up duration and τ_d controls the decay rate. The parameters are determined by enforcing (i) continuity at t_p, (ii) the peak value $P_{\max}$, and (iii) impulse matching: $I = \frac{1}{2} \cdot P_{\max} \cdot \tau_r + P_{\max} \cdot \tau_d \cdot \left(1 - e^{-(t_{end} - t_p)/\tau_d}\right)$. Given $P_{\max}$, I, t_p, t_{end}, one may either fix τ_r based on the observed rise time and solve for τ_d, or vice versa. This hybrid formulation allows one to explicitly control the pre-peak and post-peak contributions to the total impulse, which is advantageous when matching vented-deflagration records with a pronounced peak followed by a

non-negligible tail.

4. Discussion

For comparative assessment, a square thin steel plate is considered with side lengths $a = b = 1000$ mm and thickness $h = 2.0$ mm. The material is structural steel, modelled with an elastic modulus $E = 210$ GPa and density $\rho = 7850$ kg/m^3. The reference yield stress is set to $f_y = 275$ MPa, while dynamic strength enhancement is accounted for through the strain-rate formulation embedded in the bilinear SDOF resistance model. The plate response is described in terms of mid-span deflection $w_z(t)$, computed via explicit time integration of the equivalent SDOF equation of motion using the calibrated load and mass factors for the square aspect ratio ($\lambda = a/b = 1$).

Using the same plate configuration, the structure is subjected to a CFD-validated "real" vented dust-deflagration pressure–time record [15] and to five equivalent pressure histories calibrated to match the same peak pressure and positive-phase impulse within the selected window, with peak-time alignment. The alternatives are TRI, RT, RF, DRF and HYB. The mid-span deflection histories, depicted in Fig. 1, show that matching only $(P_{\max}, I)$ is not sufficient when the effective load duration and rise/decay characteristics are not negligible compared to the structural period. RT suppresses post-peak forcing (instantaneous drop at t_p), shifting the forced-to-free transition and altering phase and amplitude of the first oscillation cycles; TRI provides a smoother forcing by distributing the impulse symmetrically, but imposes an unrealistic symmetric decay, leading to deviations in envelope and timing. RF better represents progressive pressurization through explicit control of the pre-peak build-up, improving agreement around the rise-to-peak and the first response cycle. DRF extends this by superimposing two RF lobes to capture shoulder/secondary features, and in this example better reproduces the oscillation envelope by retaining part of the impulse in a delayed secondary contribution. HYB combines a realistic rise segment with a tailored post-peak decay representative of vent-driven relaxation and shows the closest overall agreement with the CFD reference, especially near the peak and during the forced-to-free transition where the response is most sensitive to the post-peak tail [16]. Overall, the 1000×1000 mm, 2 mm steel plate example indicates that equivalent loads for vented dust deflagrations should not be selected on impulse equivalence alone: rise time, peak-time alignment, post-peak relief representation, and possible secondary features can materially affect the predicted mid-span deflection demand.

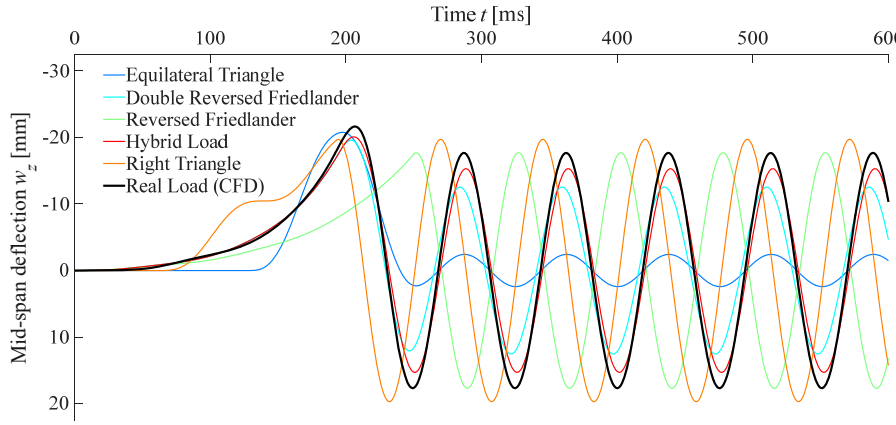

Fig. 1. Mid-span deflection histories predicted by the bilinear SDOF model under the CFD reference pressure record and the five peak- and impulse-matched equivalent load shapes

ISSN PRINT 2345-0533, ISSN ONLINE 2538-8479

5. Conclusions

An SDOF plate model with bilinear resistance and strain-rate-dependent yield strength provides a fast yet mechanically grounded framework to compare equivalent vented-deflagration loads in terms of structural demand. The present example shows that, even under peak-and-impulse matching and peak-time alignment, the mid-span response remains sensitive to load shape when the effective duration is not negligible relative to the structural response time. In such cases, impulse-only simplified representations may lead to inaccurate displacement predictions. Among the simplified laws, triangular-only pulses (RT and TRI) may misrepresent both timing and oscillation amplitude because they lack a physically meaningful post-peak relief mechanism. Reversed-Friedlander-based laws improve realism for progressive pressurization, while DRF and HYB are more suitable when the record includes secondary features or a non-negligible vent-controlled decay tail. For rapid engineering assessment of panels under vented deflagration loading, low-parameter equivalent loads should therefore control both rise and decay. The same framework can be extended to other plate-like systems and boundary conditions, and future work should address broader validation against experiments and higher-fidelity models.

Acknowledgements

The authors have not disclosed any funding.

Data availability

The datasets generated during and/or analyzed during the current study are available from the corresponding author on reasonable request.

Conflict of interest

Prof. Marco Simoncelli is a scientific committee member of the 75th International Conference on Vibroengineering and was not involved in the editorial review and/or the decision to publish this article.

References

[1] F. Pinna, M. Zucca, M. Simoncelli, and F. Stochino, "Explosion venting in dust collectors: A critical review of standards for reduced pressure and reaction force duration," *Journal of Loss Prevention in the Process Industries*, Vol. 97, p. 105670, Oct. 2025, https://doi.org/10.1016/j.jlp.2025.105670

[2] B. K. Donaldson, *Introduction to Structural Dynamics*. New York: Cambridge University Press, 2006, pp. 213–214, https://doi.org/10.1017/cbo9780511618086

[3] P. R. Amyotte and R. K. Eckhoff, "Dust explosion causation, prevention and mitigation: an overview," *Journal of Chemical Health and Safety*, Vol. 17, No. 1, pp. 15–28, Jan. 2010, https://doi.org/10.1016/j.jchas.2009.05.002

[4] R. K. Eckhoff, "Understanding dust explosions. The role of powder science and technology," *Journal of Loss Prevention in the Process Industries*, Vol. 22, No. 1, pp. 105–116, Jan. 2009, https://doi.org/10.1016/j.jlp.2008.07.006

[5] F. Rizzo, "Investigation of the time dependence of wind-induced aeroelastic response on a scale model of a high-rise building," *Applied Sciences*, Vol. 11, No. 8, p. 3315, Apr. 2021, https://doi.org/10.3390/app11083315

[6] T. Ngo, P. Mendis, A. Gupta, and J. Ramsay, "Blast loading and blast effects on structures – an overview," *Electronic Journal of Structural Engineering*, No. 1, pp. 76–91, Jan. 2007, https://doi.org/10.56748/ejse.671

[7] A. M. Remennikov, "A review of methods for predicting bomb blast effects on buildings.," *Journal of battlefield technology*, Vol. 6, No. 3, pp. 5–10, 2003.

[8] D. Cormie, G. Mays, and P. Smith, *Blast Effects on Buildings*. Thomas Telford Publishing, 2015, https://doi.org/10.1680/beob2e.35218.fm

[9] J. M. Dewey, "The friedlander equations," in *Shock Wave and High Pressure Phenomena*, Cham: Springer International Publishing, 2017, pp. 37–55, https://doi.org/10.1007/978-3-319-70831-7_3

[10] F. Pinna and F. Stochino, "Nonlinear SDOF model for dynamic response and fragility analysis of steel plates under blast loads," *European Journal of Environmental and Civil Engineering*, Vol. 29, No. 14, pp. 3048–3071, Oct. 2025, https://doi.org/10.1080/19648189.2025.2508209

[11] G. Carta and F. Stochino, "Theoretical models to predict the flexural failure of reinforced concrete beams under blast loads," *Engineering Structures*, Vol. 49, pp. 306–315, Apr. 2013, https://doi.org/10.1016/j.engstruct.2012.11.008

[12] G. R. Cowper and P. S. Symonds, "Strain hardening and strain rate effect the impact loading of cantilever beams," Brown University, Division of Applied Mathematics Report, Sep. 1957, https://doi.org/10.21236/ad0144762

[13] United States Department of Defense, *Structures to Resist the Effects of Accidental Explosions*, UFC 3-340, Unified Facilities Criteria, 2008.

[14] D. Hyde, "ConWep – Application of TM 5-855-1. Fundamentals of protective design for conventional weapons," Structural Mechanics Division, Structures Laboratory, USACE Waterways Experiment Station, 1992.

[15] F. Pinna, M. Zucca, M. Simoncelli, and F. Stochino, "A new logarithmic congestion model for vent sizing and reduced pressure prediction in baghouse dust collectors," *Journal of Loss Prevention in the Process Industries*, Vol. 99, p. 105829, Jan. 2026, https://doi.org/10.1016/j.jlp.2025.105829

[16] G. Mays and P. D. Smith, *Blast Effects on Buildings. Design of Buildings to Optimize Resistance to Blast Loading*. Emerald Publishing, 1995.